Experimental Molecular Dynamics of an Alanine-Based Helical Peptide Determined by Spin Label Electron Spin Resonance†

Siobhan M. Miick, Karen M. Casteel, and Glenn L. Millhauser*

Department of Chemistry and Biochemistry, University of California, Santa Cruz, California 95064

Received February 3, 1993; Revised Manuscript Received May 27, 1993

ABSTRACT: The alanine-based 3K(I) peptide is reported to be very helical in aqueous solution. We have prepared a series of six nitroxide spin labeled analogs of the 3K(I) sequence and measured the variable-temperature ESR spectra for each in order to reveal the position-dependent peptide dynamics. From analysis of these local dynamics under helix-forming conditions at 1 °C, we find that the helix termini show greater local dynamics than the peptide center. Further, the C-terminus is more mobile than the N-terminus. Even in the helix-promoting solvent trifluoroethanol, the results indicate that there is still substantially greater dynamics at the helix termini than at the peptide center. The unfolded state is also investigated, and we find that the peptide unfolded by guanidine hydrochloride is somewhat different than that found for high-temperature aqueous solution. Recently it was suggested that short 16-mer peptides may adopt a 3_{10}-helix structure instead of the expected α-helix. The data presented here at 1 °C show that there is sufficient disorder within the peptide to accommodate the 3_{10} structure. Also calculated are the backbone torsional fluctuations, and the results compare well to those from computer molecular dynamics studies. A proposal is outlined that explains how the enhanced dynamics found at the C-terminus results from the exposure of the helix hydrogen bonds to aqueous solvent in this region of the peptide.

The study of helix-forming peptides has emerged as a focal point in the field of protein folding [for a recent review, see Scholtz and Baldwin (1992)]. The intense interest in this area of research arises from the implicit belief that solving the protein folding problems requires a detailed understanding of the principles responsible for simple helix formation. The helix→coil transition, first described in the 1950s, is the most deeply understood transition for secondary structure in proteins (Schellman, 1958; Zimm & Bragg, 1959; Qian & Schellman, 1992). Nevertheless, the discovery of short helix-forming peptides, just within the last few years, emerged as a dramatic surprise (Marqusee & Baldwin, 1987; Marqusee et al., 1989).

The subject peptide of this present work has the alanine-based sequence:

$$\text{Ac-AAAAKAAAAKAAAAKA-NH}_2$$

and is designated as 3K(I) (A, Ala; K, Lys). First designed and synthesized by Baldwin and co-workers (Marqusee et al., 1989), the 3K(I) in aqueous solution at 1 °C gives a strong circular dichroism (CD) signal characteristic of an α-helix. It is estimated that the helix content at this temperature is approximately 70%. The CD signal decreases from increasing temperature as well as from the addition of denaturant. This peptide serves as an excellent model for probing molecular aspects of the helix→coil transition in a helix with length similar to that found in solution protein domains.

The helical 3K(I) and related peptides have received considerable scrutiny within the last few years, and it now appears that the helix→coil story is much more complicated than once thought. For instance, some experiments suggest that high helix content arises from the helix-forming tendency of Ala (Chakrabartty et al., 1991; Creamer & Rose, 1992), which may have been underestimated in host–guest experiments, whereas other studies counter this (Kemp et al., 1991). Most recently, energy calculations have suggested that the charged Lys^+ residues are responsible for helicity in Ala-based peptides (Vila et al., 1992). Even more basic, there is controversy as to the actual structure of 3K(I). Until recently it was assumed that helical peptides would only adopt an α-helix geometry (with $i \rightarrow i + 4$ hydrogen bonding). However, in our laboratory, we have shown that the 3K(I) probably follows a 3_{10}-helix geometry (with $i \rightarrow i + 3$ hydrogen bonding) or possibly an admixture of the two helix conformations (Miick et al., 1992).

Here we investigate the local peptide dynamics using spin label electron spin resonance (ESR)—a method that is ideally suited for probing dynamics on the nanosecond time scale (Nordio, 1976; Millhauser, 1992). We report on a series of 3K(I) analogs where each analog contains a single Ala→Cys (C) substitution for the specific attachment of a methanethiosulfonate spin label (MTSSL) (Todd & Millhauser, 1991):

$$\text{Ac-ACAAKAAAAKAAAAKA-NH}_2 \quad \text{(3K-2)}$$

$$\text{Ac-AAACKAAAAKAAAAKA-NH}_2 \quad \text{(3K-4)}$$

$$\text{Ac-AAAAKAACAKAAAAKA-NH}_2 \quad \text{(3K-8)}$$

$$\text{Ac-AAAAKAAAAKCAAAKA-NH}_2 \quad \text{(3K-11)}$$

$$\text{Ac-AAAAKAAAAKAACAKA-NH}_2 \quad \text{(3K-13)}$$

$$\text{Ac-AAAAKAAAAKAAAAKC-NH}_2 \quad \text{(3K-16)}$$

The designation for each peptide refers to the position of the spin label. Labeling positions were chosen to investigate local dynamics every two or three positions along the peptide sequence (except between positions 4 and 8), and only Ala residues were substituted.

In past work we reported on the 3K-4 and 3K-8 peptides (Miick et al., 1991). We showed that introduction of the Cys followed by spin labeling had only a small influence on the peptide helicity as determined by CD. We followed the local dynamics of the two peptides through the temperature-controlled helix→coil transition, and at the middle of the

† This work was supported by a grant from the National Institutes of Health (GM46870).

* Corresponding author.

0006-2960/93/0432-8014$04.00/0

transition, we found that the 3K-4 exhibited increased dynamics over the 3K-8—a finding that indicates fraying of the helical structure near the N-terminus. In a subsequent study, we directly measured the spin relaxation times with electron spin echo spectroscopy, and we showed that properly calibrated continuous wave techniques (which are used here) give an accurate and convenient estimate of the rotational correlation time for peptides in aqueous solution (Miick & Millhauser, 1992).

This present investigation of the 3K-2 through 3K-16 peptides now provides a more thorough description of the local dynamics in a helical peptide, and new features are revealed that were not seen in our initial studies of 3K-4 and 3K-8. We have recorded ESR spectra for each labeled peptide under a range of conditions including variable-temperature, influence of guanidine hydrochloride (Gu·HCl), and influence of trifluoroethanol (TFE). For each particular experimental condition, we derive a graph of local volume (V_L) vs position, which reveals the local dynamics at the labeled sites.

We find that all of the labeled peptides are very helical at 1 °C, according to CD, and they closely follow the behavior found for the parent 3K(I). In ESR experiments at 1 °C, only residues 4–11 show the uniform dynamics expected for a well-formed helix. We find that both helix ends exhibit more motional dynamics than the helix center and, interestingly, the C-terminus appears to be substantially more mobile than the N-terminus. As the temperature is raised, the observed dynamics increase throughout the peptide. Gu·HCl unfolds these short helices, and the local dynamics is found to be consistent with an unfolded peptide in solution. TFE, on the other hand, increases helicity according to CD, and TFE titrations are often used to generate a putative 100% helix reference state (Marqusee et al., 1989). We find, however, that in 20 mol % TFE the helix ends are still significantly frayed. These findings are discussed in light of the potential controversy surrounding helix geometry (3_{10} vs α), and a mechanism is also proposed to explain the enhanced dynamics of the C-terminus.

MATERIALS AND METHODS

Peptide Synthesis, Purification, and Spin Labeling. The 3K-2, 3K-11, 3K-13, and 3K-16 analogs were synthesized by Fmoc solid-phase peptide synthesis of a Rainin PS3 peptide synthesizer. The peptides were synthesized as C-terminal amides using a 4-(2′,4′-dimethoxyphenyl-Fmoc-aminomethyl)phenoxy (Rink) resin and finally capped at the N-terminus with acetic anhydride. The peptides were cleaved from the resin with a mixture of 90% trifluoroacetic acid (TFA)/5% thioanisol/5% anisol or 90% TFA/5% triethylsilane/5% anisol and crystallized from ether. Dithiothreitol was added to the samples to eliminate disulfide formation. The peptides were first purified by gel filtration chromatography on a Sephadex G-10 column in 10 mM ammonium acetate, pH 4.7, and then by reversed-phase HPLC with a C18 resin using a gradient of 5–45% acetonitrile/H_2O in 0.1% TFA and then dried under vacuum and stored at −10 °C. The peptides were reconstituted in 5 mM MOPS, pH 7, and were spin labeled at the cysteine residue by a disulfide linkage with the methanethiosulfonate spin label (MTSSL, purchased from Reanal, Hungary) by addition of MTSSL in acetonitrile in 10-fold excess to a final 5% acetonitrile-buffered solution. The reaction mixture was subsequently purified by HPLC to obtain pure spin-labeled peptide. Molecular weights for the unlabeled and labeled peptides were verified by fast atom bombardment mass spectrometry and agreed with the expected values to within

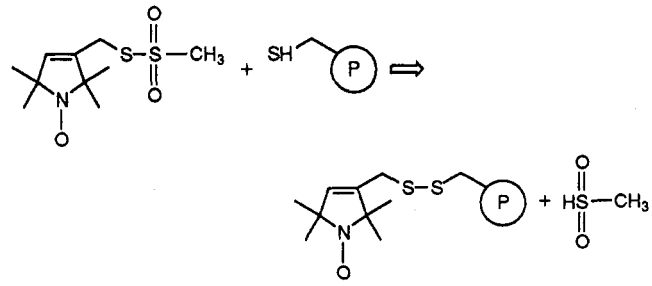

1 amu. The 3K-4 and 3K-8 were purchased from the American Peptide Company and were spin labeled in the same manner as above. ESR and CD samples were rechecked by HPLC to insure that they contained no unlabeled peptide.

Circular Dichroism. The circular dichroism spectra were acquired under temperature-controlled conditions for each of the peptides in 5 mM MOPS buffer (pH 7.1) at peptide concentrations in the range of 50–150 μM. The measurements were made on an Aviv 60DS spectropolarimeter calibrated with (+)-10-camphorsulfonic acid. The samples contained at least 100 μL of sample in a 0.1-cm path length cuvette. The peptide concentration was determined by double integration of ESR spectra and comparison to a 1 mM 4-hydroxy-TEMPO standard solution. The peptide concentrations are accurate to 5%.

Viscosity Determination. The viscosities of aqueous 6 M Gu·HCl and aqueous 20 mol % TFE at 22 °C were measured with a Cannon viscometer after calibration with water.

Electron Spin Resonance. Continuous-wave ESR spectra of the six spin-labeled peptides were acquired from samples with peptide concentrations of 0.3–1.8 mM in 5 mM MOPS buffer at pH 7.1. The ESR spectra did not vary in the concentration range studied. The measurements were made on a Bruker ESP 380 equipped with a TE_{102} rectangular cavity and operating in the continuous-wave mode. The modulation frequency was 100 kHz and the amplitude was 0.19 G. Temperature control was maintained with a Bruker variable-temperature accessory, and spectra were gathered over a 50-G scan width. Rotational correlation times, τ_R, and therefore local volumes, V_L, were determined using the same methods that we employed in our previous work [see eqs 2–4 in Miick et al. (1991)]. These values are reproducible to within a relative error of 2%.

RESULTS

Circular Dichroism. The CD spectra for each of the spin-labeled peptides exhibit minima at 208 and 222 nm, which is the characteristic signature for helical secondary structure (data not shown). The mean residue ellipticity at 222 nm, $-[\theta]_{222}$, is a sensitive measure of helix content and is plotted for the six spin-labeled peptides as a function of temperature in Figure 1. The peptides show a large, reversible decrease in mean residue ellipticity as the temperature is increased from 1 to 61 °C (see Figure 1), as was observed for the original 3K(I) (Marqusee et al., 1989). At high temperature, $-[\theta]_{222}$ values for all of the peptides appear to coalesce to a common value of approximately 6000 deg cm^2 dmol^{-1}. The original 3K(I) at 1 °C gave $-[\theta]_{222}$ = 25 000 deg cm^2 dmol^{-1}, and this value matches those found for the 3K-8, 3K-11, and 3K-16 peptides. The remaining three peptides actually give higher helicities of approximately 30 000 deg cm^2 dmol^{-1}. None of our peptides fall below the CD values found for 3K(I), and this indicates that incorporation of the Cys-MTSSL group does not significantly perturb the helical structure. For the small differences in CD signal that are observed, we can

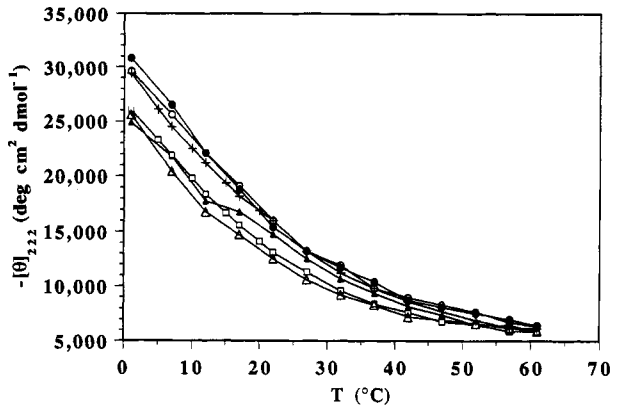

FIGURE 1: Circular dichroism mean residue ellipicity at 222 nm, $-[\theta]_{222}$, as a function of temperature for the six spin-labeled peptides: 3K-2 (○); 3K-4 (+); 3K-8 (□); 3K-11 (△); 3K-13 (●); 3K-16 (▲).

speculate that the slightly reduced helicity found for the 3K-11 and -16 relative to the 3K-2, -4, and -13 may arise from steric interactions between the spin labels and the Lys^+ residues at positions 10 and 15, respectively. The 3K-8 may be influenced by a small perturbation from the label in the center of the peptide where short helices are usually the most structured (see below).

Electron Spin Resonance. We have discussed extensively in our previous work how ESR spectra are used to reveal local dynamics for spin-labeled peptides (Todd & Millhauser, 1991; Millhauser, 1992), and we briefly review the essential points here. ESR spectra give the rotational correlation time τ_R detected by the spin label. If the spin label is rigidly attached to the peptide, and the peptide itself is rigid, then the measured τ_R will reflect the correlation time for reorientation of the entire peptide–label complex. However, if the label exhibits motion relative to the peptide, either from side-chain motion of the label or from peptide backbone motion where the label is attached, then the measured τ_R will be reduced compared to that expected for a rigid peptide–label complex. This additional motion must occur in a time comparable to or more rapid than the correlation time for the peptide, and this is approximately 0.8 ns for a 16-mer at 1 °C. Thus, ESR spectra reflect both the overall peptide motion as well as the additional motion of the labeled side chain with respect to the peptide, providing this additional motion is on the nanosecond time scale. It can be difficult to quantitatively interpret data from a single labeled peptide. However, by comparing a series of homologous peptides, observed differences must arise from variations of the motional dynamics at labeled locations on the peptide.

Direct interpretation of correlation times is hampered in both variable-temperature and variable-solvent studies because the solvent properties, such as viscosity, are changing along with the peptide dynamics of interest. In the Stokes–Einstein relation for isotropic rotational diffusion, the only parameter that directly reflects the peptide characteristics is V, the volume. This motivates a rearrangement of the Stokes–Einstein relation to

$$V_L = \frac{kT\tau_R}{\eta} \quad (1)$$

where k is the Boltzmann constant, T is the absolute temperature, and η is the solution viscosity. We refer to V_L, with units of Å^3, as the local volume, and this parameter reflects the hydrodynamic tumbling volume sensed by the spin label. This parameter is directly proportional to τ_R and reflects the local peptide dynamics. For example, considering again the

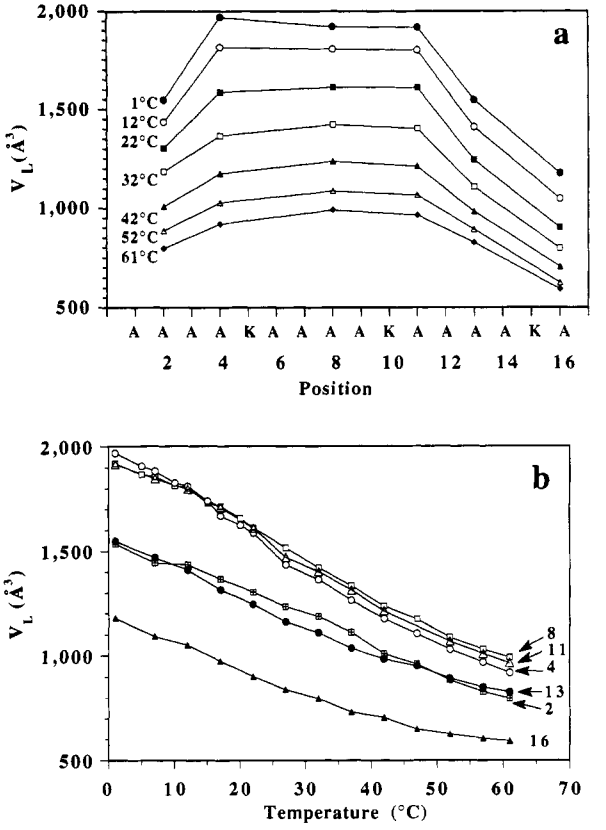

FIGURE 2: (a) Local volume, V_L, shown at each indicated temperature as a function of position for the six spin-labeled peptides. The reduced values for V_L near the ends of the peptide indicate an increase in the local dynamics. (b) Local volume, V_L (Å^3), as a function of temperature for the six spin-labeled peptides.

example of a label rigidly attached to a rigid peptide, V_L will give the solvated hydrodynamic volume of the entire peptide–label complex. This value will be the upper bound for a monomeric peptide. If there are additional nanosecond dynamics of the label relative to the peptide, then V_L will have a reduced value. Thus, the presence of position-dependent backbone dynamics will give rise to variations in V_L when comparing the series of labeled peptides in this study.

ESR data were acquired for each of the six peptides over the temperature range of 1–61 °C. The nitroxide spectra for each of the spin-labeled peptides did not show any concentration dependence over the range of 300 μM to 2 mM. From these ESR spectra, V_L was determined for each peptide as a function of temperature. We did not find evidence of anisotropic motion (Todd & Millhauser, 1991), so the V_L's were computed from eq 1. Figure 2a is a plot of V_L vs label position at each temperature. At 1 °C the highest V_L's are between positions 4 and 11 and the V_L's are uniform in this region. Moving to the end positions of the helix, we see that the 3K-2, 3K-13, and 3K-16 peptides all show reduced V_L values, which indicates that these positions exhibit greater motional dynamics. This is readily seen in Figure 2b, which shows the data from Figure 2a now plotted for each label position vs temperature. Comparing the 3K-4 and the 3K-13, where the label is the same number of residues from the respective nearest ends of the peptide, one can see a considerable difference in V_L of 400 Å^3. Furthermore, the 3K-16 gives a lower V_L than the 3K-2. These data indicate that the C-terminus is substantially more mobile than the N-terminus, i.e., the C-terminus is more frayed than the N-terminus. These differences will be addressed in the Discussion section.

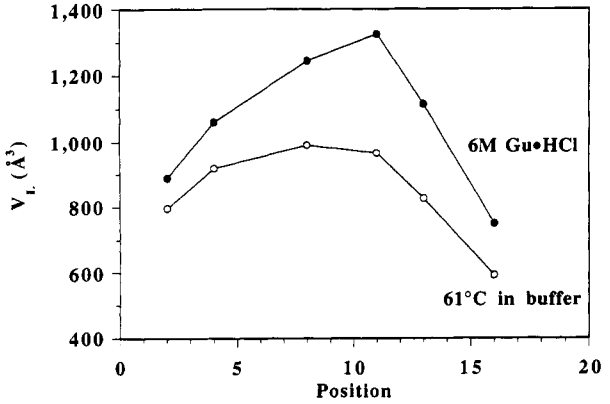

FIGURE 3: V_L as a function of position for peptides unfolded by high temperature in buffered aqueous solution and by denaturant of 6 M Gu·HCl at 22 °C.

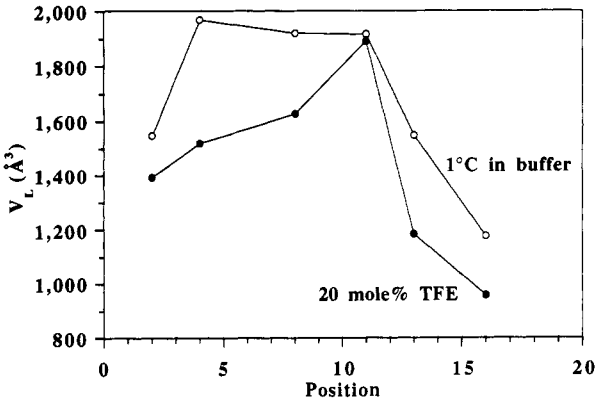

FIGURE 4: V_L as a function of position for peptides under helix-forming conditions of low temperature in buffered aqueous solution and 20 mol % TFE at 22 °C.

As the temperature is increased, V_L monotonically decreases for each labeled position, which indicates an increase in the overall peptide dynamics. At 32 °C and above, V_L is no longer uniform in the peptide center and the 3K-8 shows the highest V_L. At all temperatures, however, the enhanced dynamics of the C-terminus is apparent. Figure 2b reveals groupings in the temperature-dependent dynamics, with the central positions 4, 8, and 11 showing similar behavior and likewise for positions 2 and 13.

To examine the chemically unfolded state, we used Gu·HCl, a common protein denaturant. V_L's extracted from the peptides in 6 M Gu·HCl and the high-temperature 61 °C data (from Figure 1) in aqueous buffer are shown in Figure 3. It is interesting to note that the V_L data in 6 M Gu·HCl are larger than those of the thermal denaturation, even after accounting for the much higher viscosity of 6 M Gu·HCl (see eq 1). In this instance, it is important to recognize that V_L partially reflects the solvation shell that orients with the spin-labeled peptide and that this shell, or cage, may contain guanidine molecules interacting with the peptide. Focusing on the shape of the V_L vs position curves in Figure 3, we note that an asymmetric distribution of the V_L values is observed in both the chemical and thermal denatured states of these peptides; however, subtle differences are seen when comparing the 3K-4 with the 3K-13. At 61 °C in buffer, the 3K-4 peptide has a V_L that is greater than the V_L for the 3K-13, whereas in 6 M Gu·HCl, the relative local volumes of these two peptides are reversed.

TFE promotes helix formation according to CD (Nelson & Kallenbach, 1986). The maximum CD signal obtained from progressive addition of TFE has been interpreted as that of the 100% helix reference state for the 3K(I) (Marqusee et al., 1989). Figure 4 shows position-dependent results for the peptides in 20 mol % TFE at 22 °C (room temperature), and these results are compared to those found at 1 °C in aqueous buffer (from Figure 2). The V_L's for TFE are, on average, smaller than those for the buffered aqueous solution. This is probably attributable either to a small decrease in the size of the solvent cage around the peptide (in contrast to what we proposed above for Gu·HCl) or to additional thermal motion in the room-temperature TFE solution. Interestingly, the V_L's do not show uniform values as one would expect for a well-formed helix—the helix ends are still quite frayed. Position 11 appears to give an unusually large V_L, and this value drops off smoothly toward the N-terminus. V_L exhibits a sudden change between positions 11 and 13, and the C-terminus is substantially more mobile than the N-terminus.

DISCUSSION

Our data clearly show that there is position-dependent nanosecond dynamics in the alanine-based 3K(I) peptide. From the variable-temperature data, we find that the helix ends are frayed and that the C-terminus ends are more so than the N-terminus ends. These data are interpreted as reflecting relative backbone motions along the peptide sequence. However, it is worthwhile considering whether the observations presented here might arise from other effects. For example, one might be concerned with the motion of the spin-labeled side chain resulting from rotations about the side-chain dihedral angles. Past work, though, has shown that MTSSL forms a fairly rigid attachment to Cys side chains (Todd & Millhauser, 1991). Furthermore, such motion would be uniform along the peptide sequence and would not give the strong position-dependent results observed here.

An alternative possibility for the observed position dependence of V_L is that side-chain motion is more prevalent at the helix termini because at these positions the spin label can extend beyond the helix ends and assume orientations that are not accessible for the central label positions. This is an unlikely explanation, though, because in a helix the side chains are directed toward the N-terminus and this would result in positions 2 and 4 giving the lowest V_L's, and this is not observed. Further, position 4 is only at the beginning of the second helical turn from the N-terminus and should exhibit more conformational freedom than positions 8 or 11. However, Figure 2 shows that at low temperature these positions give nearly equivalent V_L's. From these arguments we conclude that differences in V_L at the various label positions reflect genuine differences in the peptide backbone motion along the sequence.

The data presented here have implications regarding the structure of short helix-forming peptides. Until recently, it has been assumed that helical peptides must adopt an α-helix conformation since this is the dominant helical form in proteins. The less common 3_{10}-helix structure [recently reviewed by Toniolo and Benedetti (1991)] was largely ignored. However, the usual techniques used to reveal structure in peptides are nuclear magnetic resonance (NMR) and CD, and these methods are unable to conclusively distinguish 3_{10} from α. To resolve this, we used Fourier transform infrared (FTIR) spectroscopy and ESR of doubly labeled peptides, and surprisingly, we found that the 3_{10}-helix was the preferred conformation (Miick et al., 1992). Our result was unexpected because analysis of X-ray crystal structures has shown that 3_{10}-helices in proteins are short and are never longer than six residues, which is two helical turns (Barlow & Thornton, 1988).

However, inspection of the data in Figure 2a at 1 °C shows that under helix-forming conditions only the center of the peptide exhibits the uniform dynamics expected for an ordered helix. This central region stretches from position 4 to position 11, to within the resolution of the chosen labeling sites, and this region is eight residues long (and less than three turns of a 3_{10}-helix). Thus, the significant fraying of the helix ends in 3K(I) may accommodate 3_{10}-helix formation in the peptide center.

Position-dependent behavior in helical peptides has been the subject of both computer molecular dynamics (MD) studies as well as several experimental investigations. MD work was performed by Daggett et al. (1991) on a 20-mer of poly(Ala) to probe the motions involved in the helix→coil transition. The trajectory was run at 400 K, and solvent was not explicitly included. Within a 4-ns trajectory, several full helix→coil transitions were observed, as were many transitions leading to partial unfolding. These data revealed a rich behavior in peptide dynamics on the nanosecond time scale with hints of local cooperativity. Position-dependent dynamics were clearly observed, as seen in the angular variance of the polypeptide dihedral angles, and the ends were clearly more dynamic than the peptide center (see below). However, little difference was seen in the dynamics of the two helix termini.

Tirado-Rives and Jorgensen (1991) also used MD to probe the unfolding of a ribonuclease S-peptide analog. Computations were for less than 500 ps, but in this case the aqueous solvent was treated explicitly. In contrast to the poly(Ala) work, this calculation did show enhanced unfolding of the C-terminus compared to the N-terminus, and this difference was attributed to the high helix propensity of three consecutive Ala's located at the beginning of the peptide sequence. Interestingly, their study found that breakage of most backbone amide hydrogen bonds proceeded through the following unfolding sequence: $\alpha \rightarrow 3_{10} \rightarrow$ no bond. Soman et al. (1991) also treated water explicitly in an MD study of the unfolding of a myoglobin α-helix. A 1-ns calculation showed that unfolding proceeded from the C-terminus to the N-terminus, with fraying of the ends occurring within the first 100 ps. They observed transient structures, including turns and helical regions, with bifurcated hydrogen bonds corresponding to a geometry between α and 3_{10}.

Experimentally, Chakrabartty et al. (1991) probed the distribution of helicity in an Ala-based peptide by systematically replacing each Ala by a helix-breaking Gly. Helicity was determined by CD, and this work showed that Gly exerted the greatest helix-breaking influence when at the peptide center, thus locating the region of greatest helix content. This effect dropped off monotonically as the Gly substitution was moved to either end of the peptide. Small differences were seen when comparing the two peptide ends where the two substituted positions closest to the C-terminus appear to reveal lower helicity than the two substituted positions closest to the N-terminus. The authors did not comment on this difference.

NMR has been used in several studies for examining position-dependent helicity in peptides. Nuclear Overhauser effects (NOEs) between specific protons (predominantly between the NH at position i and the C_α proton at position $i+3$) as well as the ϕ-dependent three-bond coupling constants, $^3J_{\alpha N}$, are diagnostic of local helix geometry. For a ribonuclease C-peptide analog, Osterhout et al. (1989) found extensive helical structure, with the N-terminus less helical than the rest of the peptide. They proposed that the N-terminus was distorted due to the formation of a salt bridge between $Glu2^-$ and $Arg10^+$. Lockhart and Kim (1992, 1993) have modified 21-residue analogs of the Ala-based subject peptide in order to measure the electric field at the N-terminus. A strong series of NOEs was used to verify that the helical residues followed a well-structured α-helix. It was asserted that the 3_{10}-helix is not significantly populated in these longer peptides.

Bradley et al. (1990) designed a heterogeneous 17-mer that showed helical structure mainly between residues 5 and 14, with the ends giving extended nonhelical structures. Interestingly, these authors estimated the total helix content based on their NMR results and proposed that the average helix population was greater than that found from their CD results. They also suggested that the limiting CD signal obtained by TFE addition was not a good reference state for 100% helix. Liff et al. (1991) designed a 21-mer helical peptide that was stabilized by a series of $Glu^-\cdots Lys^+$ salt bridges. The center of the peptide contained three consecutive guest residues which had been used to rank helix propensities (Lyu et al., 1990). NMR work showed that helicity was largely skewed toward the N-terminus, with a maximum near position 8. They also found that addition of TFE did not produce a 100% helical state. Most recently, Storrs et al. (1992) used an S-peptide analog, covalently initiated at the N-terminus, to isolate the effect of TFE on helix propagation. While 50 vol % TFE was found to substantially increase helix content, their NMR data did reveal that the C-terminus remained disordered.

The MD, Gly substitution, and NMR investigations above all indicate that fraying at the termini is always present in peptide helices, and when the two termini are not equally disordered, the C-terminus is more frayed than the N-terminus. The only exception to this was seen by NMR of the C-peptide analog in which lack of structure at the N-terminus was explained by a specific salt-bridge interaction.

To compare our data with findings from other labs, it is important to point out how our measurements differ in perspective. NMR reveals structure through interproton distances and dihedral angles. The Gly substitution experiments probe the influence of a helix breaker on the helix–coil equilibrium. In contrast, our experiments reveal the motional dynamics. To appreciate the difference, consider a helical peptide that is rigid and yet unstructured at the two termini. This case would give uniform motional dynamics (and therefore uniform V_L's), whereas NMR would indicate a loss of structure at the termini. One might refer to this case as "static fraying" of the helix ends. The work presented in this article reveals the "dynamic fraying" of the helix ends. It is interesting that our results agree qualitatively with those from the studies discussed above. Thus, where there is static fraying there is also dynamic fraying, and so a loss of local structure means an increase of local dynamics on the nanosecond time scale.

Our results from the 3K(I) in TFE also concur with structural studies. As mentioned above, addition of TFE to 20 mol % (approximately 50% v/v) increases the CD signal for the 3K(I) to a maximum. NMR, though, has shown that addition of TFE does not produce a uniformly helical peptide in those that have been studied and that the peptide ends remain unstructured. Our findings shown in Figure 4 indicate that there also remains significant dynamic fraying of the helix ends, especially at the C-terminus, in 20 mol % TFE.

Providing a quantitative interpretation of our position-dependent dynamics data is challenging because V_L contains contributions from both the time scale of the backbone motion and well as the amplitude of this motion. Additionally, the MD work discussed above has shown that there are probably many different types of motions involved in peptide structural fluctuations. Nevertheless, we can use simplifying but

reasonable approximations to give a semiquantitative estimate of the backbone torsional fluctuations. As suggested by MD calculations, backbone motions can give small fluctuations within tens of picoseconds. Thus, we can assume that these fluctuations are rapid and independent of overall peptide reorientation, and we can apply the model-free approach (Lipari & Szabo, 1982). This theory states that, when a spin attached to a macromolecule experiences rapid local motion, spectral densities

$$j(\omega) = \frac{\tau_R}{1 + \tau_R^2\omega^2} \tag{2}$$

in T_1 and T_2 relaxation expressions must be replaced with

$$j(\omega) = \frac{S^2\tau_R}{1 + \tau_R^2\omega^2} + (1 - S^2)\tau_e \tag{3}$$

where τ_R is the rotational correlation time of the macromolecule and τ_e is the correlation time for local fluctuations. S is an order parameter that is related to the amplitude of local motion. For instance, if the spin is perfectly ordered within the frame of the macromolecule and does not experience local motion, then $S = 1$ and eq 3 reduces to eq 2. Conversely, if the spin experiences unrestricted local motion, then $S = 0$ and the spectral density is dominated by the correlation time for local motion.

Using eq 3 with the motional narrowing spin relaxation theory for nitroxide spin labels (Goldman et al., 1972; Todd & Millhauser, 1991), the observed correlation time becomes

$$\tau_{R,obs} = S^2\tau_{R,peptide} + (1 - S^2)\tau_e \tag{4a}$$

$$\tau_{R,obs} \cong S^2\tau_{R,peptide} \tag{4b}$$

where $\tau_{R,obs}$ is the experimentally observed correlation time and $\tau_{R,peptide}$ is the hypothetical peptide rotational correlation time in the absence of local motion. In eq 4b we have assumed that $(1 - S^2)\tau_e \ll S^2\tau_{R,peptide}$. Using eq 1 we now have

$$V_{L,obs} = S^2V_{L,peptide} \tag{5}$$

where $V_{L,obs}$ and $V_{L,peptide}$ are the hydrodynamic volumes sensed by the spin label in the presence and in the absence of local motion, respectively.

Several models are commonly used for the interpretation of S, and perhaps the most simple one is the cone model in which the backbone allows for unrestricted motion of the label to within an angle of θ_o away from the mean position (Lipari & Szabo, 1982; Campbell & Dwek, 1984). This angle of movement for each position is calculated with

$$\theta_o = \cos^{-1}\left[\frac{\sqrt{1 + 8S} - 1}{2}\right] \tag{6}$$

where S is the order parameter calculated at each position from eq 5.

Equations 5 and 6 now provide a means for estimating the extent of local torsional motion. However, we first need to determine $V_{L,peptide}$, which is, in principle, a hypothetical value that cannot be directly measured in our experiments since there is always some degree of motion at each labeled position. In previous work, we have addressed the expected value for V_L given the approximate dimensions of a rigid 16-mer helix and $T = 1$ °C, and we estimated $V_L = 2000$ Å^3 (Miick et al., 1991). Inspection of the data taken at 1 °C in Figure 2a shows that between positions 4 and 11 the peptide dynamics are uniform and exhibit less motion than the peptide ends and that position 4 gives the highest V_L. Thus, $V_{L,peptide}$ should

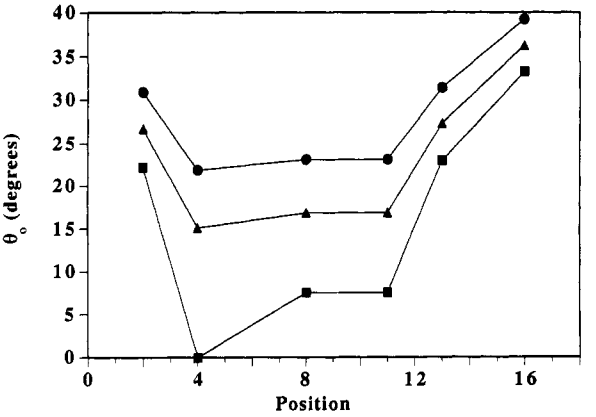

FIGURE 5: Angle of torsional motion, θ_o, vs position for three values of $V_{L,peptide}$ as calculated from the cone model (see eqs 5 and 6) using the data at 1 °C from Figure 2a: $V_{L,3K-4} = V_{L,peptide}$ (■); $V_{L,3K-4} = 0.9V_{L,peptide}$ (▲); $V_{L,3K-4} = 0.8V_{L,peptide}$ (●).

be only slightly larger than that found for the 3K-4. In Figure 5 we explore this by computing θ_o vs position from the data at 1 °C for three cases where we take $V_{L,3K-4} = V_{L,peptide}$, $V_{L,3K-4} = 0.9V_{L,peptide}$, and $V_{L,3K-4} = 0.8V_{L,peptide}$. Between positions 4 and 11 we find that θ_o is conservatively calculated to be between 5° and 25°, depending on the choice of $V_{L,peptide}$. At both peptide termini, θ_o increases and a maximum value is seen for position 16 between 33° and 39°. We note that θ_o is not very sensitive to the choice of $V_{L,peptide}$, and this is revealed by evaluation of eqs 5 and 6 which shows that cos θ_o is proportional to $(V_{L,peptide})^{-1/4}$. Thus, to within the approximation of the cone model, the calculations shown in Figure 5 provide a good representation of the torsional motion sensed at each labeled position in the peptide.

MD work for α-helical poly(Ala) (Daggett et al., 1991) found that the peptide backbone dihedral angles exhibit torsional fluctuations with $\langle\delta\phi\rangle \approx \langle\delta\psi\rangle \approx 12$–$14°$ throughout the center of the peptide. About four positions from either end of the peptide, these fluctuations suddenly increase and reach maximum values at the peptide ends of approximately 30°. Our data in Figure 5 match these MD findings surprisingly well. Of course, it is not known at this time whether MD would give different results for a 3_{10}-helix. We are encouraged, though, that there is semiquantitative agreement between computer molecular dynamics and the experimental dynamics sensed by spin labels. Further work is needed, but these calculations show that spin label ESR will provide an important benchmark for calibrating MD calculations on peptides.

Finally, we address the enhanced dynamic fraying found at the peptide termini and, specifically, why the C-terminus apparently exhibits more motional dynamics than the N-terminus. Both ends of the peptide are capped, which should eliminate helix-destabilizing charge–macrodipole interactions (Scholtz & Baldwin, 1992). One obvious asymmetry between the two helix ends is the Lys^+ at position 15 near the C-terminus. Lys^+ has, tentatively, a lower helix propensity than Ala, and this may lead to disorder in this region of the peptide. However, basic side-chain groups are often helix-stabilizing when near the C-terminus (Richardson & Richardson, 1988), so that it is difficult at this juncture to know whether the helical content is lower or higher at the C-terminus.

We would like to approach this problem from a different perspective by noting that in all capped helical peptides there is an intrinsic structural difference between the first sequential hydrogen bond (H-bond) formed at the N-terminus and the last sequential H-bond formed at the C-terminus. This

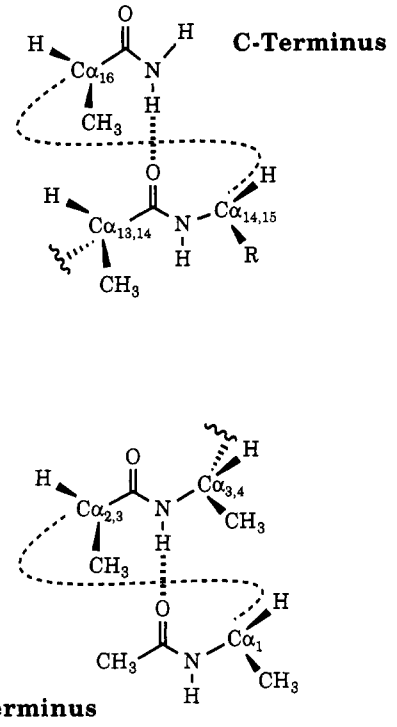

FIGURE 6: N-terminus and C-terminus backbone hydrogen bonds showing the local environments. At the N-terminus, the first hydrogen bond is formed between the C=O of the capping group and the peptide bond NH of either the 3rd or 4th residue, depending on α- or 3_{10}-helix conformation. The C-terminus forms the last hydrogen bond between the C=O of the 13th or 14th residue, depending on helix conformation, and the NH_2 capping group. The N-terminus hydrogen bond is protected by amino acid side chains, whereas the C-terminus hydrogen bond is more exposed to the solution.

difference is in the local steric environment and arises from the orientation of the helix side chains which are directed toward the N-terminus in L-amino acids. The first and last possible helix backbone H-bonds are diagrammed in Figure 6. At the N-terminus, the first possible H-bond is formed between the C=O of the acetyl capping group and the NH of either residue 3 or 4, depending upon whether the helix is 3_{10} or α. From the two C_α's on either side of the NH, the CH_3 side chains point toward the N-terminus and provide steric protection for the H-bond from the aqueous solvent. At the C-terminus the situation is quite different. The last possible H-bond is formed between the NH_2 capping group and the C=O of either residue 13 or 14, depending on helix conformation. Here the only steric protection is from the side chain of residue 16. The side chains flanking the C=O acceptor point away from the H-bond and do not provide steric protection. Although the N-terminus vs C-terminus asymmetry is described here in terms of the first and last possible peptide H-bonds, this difference would also exist in any helical domain within a longer peptide or protein.

From this analysis, we believe that the enhanced dynamics seen at the C-terminus may not necessarily reflect a loss of H-bond energy in this region of the peptide. Indeed, the H-bonds at either end of the helix may have equal strength. However, when a helix H-bond breaks, new bonds must be formed by both the donor and the acceptor to the aqueous solvent. Crystallographic studies of proteins have shown that C=O groups in helix H-bonds are often bifurcated to H_2O, and this usually leads to local distortion (Baker & Hubbard, 1984). Recently solved structures of short helical peptides have provided direct evidence that water can insert between the donor and acceptor of a helical H-bond at the C-terminus (Karle et al., 1990). This structural evidence suggests that the last C-terminus H-bond is more exposed to solvent and this may allow H-bond breakage to occur with less distortion and lower activation energy and, hence, much more rapidly than at the N-terminus. Then, once an H-bond is broken at a helix terminus, the next sequential H-bond is left exposed to solvent. Therefore, we propose that the enhanced dynamic fraying of the C-terminus arises from exposure to solvent and, consequently, the low activation energy of H-bond breakage in this unique location in the helix.

CONCLUSION

It appears that helical peptides still present unexpected behavior that challenges the present understanding of peptide and protein structure and dynamics. It is gratifying that the results presented here for local backbone torsional fluctuations approximately match the results from computer molecular dynamics. On the other hand, more work is needed to determine whether enhanced dynamic fraying of the C-terminus is an intrinsic property of all helical peptides or only a special case of the 3K(I). We also expect that there is still controversy regarding the actual helix geometry—3_{10} vs α—and we believe that the data presented here show that a 3_{10} structure is certainly possible since only the peptide center shows uniform order.

ACKNOWLEDGMENT

We thank Professor Sheila David for helpful comments on the manuscript.

REFERENCES

Baker, E. N., & Hubbard, R. E. (1984) *Prog. Biophys. Mol. Biol. 44*, 97–179.

Barlow, D. J., & Thornton, J. M. (1988) *J. Mol. Biol. 201*, 601–619.

Bradley, E. K., Thomason, J. F., Cohen, F. E., Kosen, P. A., & Kuntz, I. D. (1990) *J. Mol. Biol. 215*, 607–622.

Campbell, I. D., & Dwek, R. A. (1984) *Biological Spectroscopy*, Benjamin/Cummings, Inc., Menlo Park, CA.

Chakrabartty, A., Schellman, J. A., & Baldwin, R. L. (1991) *Nature 351*, 586–588.

Creamer, T. P., & Rose, G. D. (1992) *Proc. Natl. Acad. Sci. U.S.A. 89*, 5937–5941.

Daggett, V., Kollman, P. A., & Kuntz, I. D. (1991) *Biopolymers 31*, 1115–1134.

Goldman, S. A., Bruno, G. V., Polnaszek, C. F., & Freed, J. H. (1972) *J. Chem. Phys. 56*, 716–735.

Karle, I. L., Flippen-Anderson, J. L., Uma, K., & Balaram, P. (1990) *Proteins 7*, 62–73.

Kemp, D. S., Boyd, J. G., & Muendel, C. C. (1991) *Nature 352*, 451–454.

Liff, M. I., Lyu, P. C., & Kallenbach, N. R. (1991) *J. Am. Chem. Soc. 113*, 1014–1019.

Lipari, G., & Szabo, A. (1982) *J. Am. Chem. Soc. 104*, 4546–4559.

Lockhart, D. J., & Kim, P. S. (1992) *Science 257*, 947–951.

Lockhart, D. J., & Kim, P. S. (1993) *Science 260*, 198–202.

Lyu, P. C., Liff, M. I., Marky, L. A., & Kallenbach, N. R. (1990) *Science 250*, 669–673.

Marqusee, S., & Baldwin, R. L. (1987) *Proc. Natl. Acad. Sci. U.S.A. 84*, 8898–8902.

Marqusee, S., Robbins, V. H., & Baldwin, R. L. (1989) *Proc. Natl. Acad. Sci. U.S.A. 86*, 5286–5290.

Miick, S. M., & Millhauser, G. L. (1992) *Biophys. J. 63*, 917–925.
Miick, S. M., Todd, A. P., & Millhauser, G. L. (1991) *Biochemistry 30*, 9498–9503.
Miick, S. M., Martinez, G. V., Fiori, W. R., Todd, A. P., & Millhauser, G. L. (1992) *Nature 359*, 653–655.
Millhauser, G. L. (1992) *Trends Biochem. Sci. 17*, 448–452.
Nelson, J. W., & Kallenbach, N. R. (1986) *Proteins 1*, 211–217.
Nordio, P. L. (1976) *General Magnetic Resonance Theory*, Academic Press, New York.
Osterhout, J., Jr., Baldwin, R. L., York, E. J., Stewart, J. M., Dyson, H. J., & Wright, P. E. (1989) *Biochemistry 28*, 7059–7064.
Qian, H., & Schellman, J. A. (1992) *J. Phys. Chem. 96*, 3987–3994.
Richardson, J. S., & Richardson, D. C. (1988) *Science 240*, 1648–1652.
Schellman, J. A. (1958) *J. Phys. Chem. 62*, 1485–1494.
Scholtz, J. M., & Baldwin, R. L. (1992) in *Annual Review of Biophysics and Biomolecular Structure* (Engelman, D. M., Cantor, C. R., Pollard, T. D., Eds.) pp 95–118, Annual Reviews Inc., Palo Alto, CA.
Soman, K. V., Karimi, A., & Case, D. A. (1991) *Biopolymers 31*, 1351–1361.
Storrs, R. W., Truckses, D., & Wemmer, D. E. (1992) *Biopolymers 32*, 1695–1702.
Tirado-Rives, J., & Jorgensen, W. L. (1991) *Biochemistry 30*, 3864–3871.
Todd, A. P., & Millhauser, G. L. (1991) *Biochemistry 30*, 5515–5523.
Toniolo, C., & Benedetti, E. (1991) *Trends Biochem. Sci. 16*, 350–353.
Vila, J., Williams, R. L., Grant, J. A., Wojcik, J., & Scherga, H. A. (1992) *Proc. Natl. Acad. Sci. U.S.A. 89*, 7821–7825.
Zimm, B. H., & Bragg, J. K. (1959) *J. Chem. Phys. 31*, 526–535.